



## Correlation between microstructure and corrosion behaviour of Bi-Zn solder alloys

Rudimylla S. Septimio <sup>a</sup>, Maria A. Arenas <sup>b</sup>, Ana Conde <sup>b</sup>, Amauri Garcia <sup>a</sup>, Noé Cheung <sup>a</sup> and Juan de Damborenea <sup>b</sup>

<sup>a</sup>Department of Manufacturing and Materials Engineering, University of Campinas, UNICAMP, Campinas, Brazil; <sup>b</sup>National Center for Metallurgical Research (CENIM-CSIC), Madrid, Spain

### ABSTRACT

Bi-Zn solder alloys with different Zn contents (1.5, 2.7 and 5wt-%) were prepared by casting and the correlation between the microstructure and corrosion behaviour by mean of direct current electrochemical tests was studied. The surface analysis of the hypoeutectic Bi-Zn alloy samples revealed the presence of needle-like ZnO and very small agglomerated spherical particles. By contrast, eutectic alloy presented the formation of a uniform and compact film of ZnO, which is related to the better distribution of Zinc in the Bi-rich matrix. Despite the increase in Zn content compared to the hypoeutectic alloy, the corrosion rate showed similar values regardless of its content in the alloy. The Bi-5wt-% Zn alloy presented the highest limiting current density, and consequently, the highest degree of corrosion of the studied alloys. The pro-eutectic phase consisting of large and thick Zn fibres is preferentially dissolved, promoting a selective attack that penetrates inside the sample.

### ARTICLE HISTORY

Received 26 December 2018  
Revised 22 March 2019  
Accepted 25 March 2019

### KEYWORDS

Solder alloys; Bi-Zn alloys; microstructure; corrosion resistance

### Introduction

Bi-based materials are of great importance in many fields such as in the pharmaceutical, chemical and semiconductors industries [1]. Owing to its excellent chemical properties, Bi has already been used as medical therapeutic agent, medicines or nontoxic dyes [2]. Over the last years, it has also been suggested for applications as a thermoelectric material [3], optical and electro-optical devices [4], hall sensors [5], hydrophobic surface [6], as well as lubricant materials [7,8].

Bismuth has also been indicated as an alternative base element for Pb-free alloys for the replacement of the traditional Sn-Pb solder alloys [9] used in electronic assemblies, because of the inherent toxicity of lead. The great challenge in developing these alternative alloys is the improvement of a specific property without promoting deleterious effects in another one. Although the mechanical strength is usually one of the main properties to be evaluated, service lifetime also depends on the corrosion behaviour when exposed to an aggressive environment.

Corrosion is a surface phenomenon that occurs spontaneously because of thermodynamic instability of all metals and alloys. When exposed to atmosphere, in particular high relative humidity with halide ions, the solders become susceptible to corrosion, which can deteriorate their long-term reliability promoting electrical discontinuity and degradation of the mechanical properties of the solder joint [10]. Since the technological advance demands increasingly performance under severe operating conditions, it becomes necessary to evaluate the new Pb-free solder alternatives in aggressive environments.

It is well known that the chemical composition, morphology and distribution of phases in the microstructure affect the corrosion resistance in any kind of alloys [11–13], whatever the main elements composing the alloy [14,15]. As an example, a recent research developed by Zhongbo

et al. [14] examined the role of microstructure features on the corrosion resistance of Zr–0.8Sn–1Nb–0.3Fe alloy sheets prepared by different heat treatment processes. They showed that corrosion resistance of such Zr-based alloys mainly depends on the size, distribution and the Nb content of second phase particles. Another work regarding the corrosion analysis of as-cast Al–Mg–Si alloy samples has shown that finer cellular and dendritic microstructural arrays are associated with lower corrosion current densities and nobler corrosion potential as compared to coarser microstructures [15].

Regarding Zn-containing alloys, it has been shown that Zn segregation affects both the microgalvanic cell and the cathode-to-anode area ratio on Mg–25 wt-% Zn alloy [16]. The authors observed that a finer and homogeneously distributed Mg-rich equiaxed dendritic grains induced lower corrosion current density compared to coarser ones. With respect to the influence of the chemical composition, Ahmido et al. [17] studied the role of alloying elements such as Ag and Bi on the corrosion resistance of a Sn–9wt-%Zn alloy in a 3 wt-% NaCl solution. The results showed that the addition of Bi and Ag leads to increase the corrosion rate as well as a shift towards less noble values of the corrosion potential ( $E_{\text{corr}}$ ).

Also on biodegradable dilute Zn–0.3wt-%Mg and Zn–0.5wt-%Mg alloys has been observed that coarser microstructures of both alloys are associated with lower corrosion resistance than finer microstructures [18]. This work analysed the corrosion behaviour of two directionally solidified samples of each alloy casting. It was shown that samples that solidified under lower cooling rates presented slightly higher corrosion kinetics as compared to pure Zn and with the samples from positions close to the cooled bottom of the castings (higher solidification cooling rates), which have finer microstructural arrays

A recent work by the present authors has examined the evolution of the microstructure of hypoeutectic, eutectic

and hypereutectic Bi-Zn solder alloys under an extensive range of cooling rates during solidification under transient heat flow conditions [19]. The analysis of the resulting microstructures permitted the identification of different phase morphologies, e.g. Bi-rich trigonal dendrites and long Zn fibres, as primary phases of, hypoeutectic and hypereutectic alloys, respectively, immersed in a fiber-like eutectic mixture. However, there is lack of information on the electrochemical corrosion behaviour of these Bi-Zn solder alloys. For a better understanding on the role of the microstructure features on the resulting corrosion behaviour it is necessary to accomplish a systematic study concerning the influence of the variation of Zn content in Bi-Zn binary alloys. Therefore, in this study, hypoeutectic, eutectic and hypereutectic Bi-Zn alloys are prepared and corrosion studies have been performed to investigate the influence of the microstructure on the corrosion resistance.

### Experimental procedure

The nominal composition of the Bi-Zn solder alloy analysed in the present work are: Bi-1.5wt-%Zn (hypoeutectic), Bi-2.7wt-%Zn (eutectic), and Bi-5wt-%Zn (hypereutectic). To prepare these solder alloys, commercially pure Bi (containing 0.0027wt-%Ag, 0.001wt-%Sn, 0.0007wt-%Pb, 0.001wt-% Cd, and <0.0001wt-% Fe) and Electrolytic Zn (containing 0.015 wt-% Fe, 0.012 wt-% Pb and 0.003 wt-% Si) were used. The electrochemical tests were also performed on pure Bi and Zn samples for comparison purposes. This analysis is required to understand what happens when these two elements, which have so different electrochemical nature/characteristics, form rich-phases that constitute the microstructure of the alloy and the influence of their sizes and distribution on the electrochemical activity of the alloy.

The alloys were produced in a water-cooled solidification setup. The details of the experimental casting apparatus, melting and solidification procedures have been described in a previous study by the authors [19].

In order to analyse microstructural features and corrosion behaviour, samples were extracted from the directionally solidified Bi-Zn cylindrical castings. The samples were ground with 100, 200, 400, 600 and 1200 grit SiC papers, and then finely polished with diamond paste (6 and 1  $\mu\text{m}$ ) for metallography. No etching was necessary for revealing the microstructure of the samples. The examination of the microstructure was carried out using an optical Olympus Invert Metallurgical Microscope (model 41 GX) and a Back Scattered Electron imaging (BSE) of a scanning electron microscopy (ZEISS-EVO-MA15), equipped with Energy Dispersive Spectrometer (EDS) (Oxford-X-MAX), was used to complement the microstructural characterisation.

For the electrochemical tests, the samples were ground with successive silicon-carbide papers up to 1200 grit, followed by polishing with a 6  $\mu\text{m}$  diamond paste, and finally ultrasonically cleaned with ethanol and dried with cold air. The electrochemical tests were performed using a Gamry Reference 600 potentiostat and conducted in triplicate. The electrochemical cell was a three-electrode cell; where an Ag/AgCl (3M KCl) electrode was the reference electrode, the counter-electrode was a platinum wire, and the working electrode was the sample under study. The used electrolyte was a 0.06 M NaCl solution, prepared from reagent grade chemicals and distilled water. The exposed area of the samples was

0.17  $\text{cm}^2$ . The volume of electrolyte used for electrochemical tests was 30 mL. All the tests were done in aerated conditions at room temperature.

Before performing the polarisation curves, the evolution of the open circuit potential (OCP) was recorded for 15 min. It was settled a scan rate of 0.16  $\text{mV s}^{-1}$  from an initial potential of  $-300 \text{ mV vs. } E_{\text{OCP}}$ , until reaching a potential of 0.8 V vs. Ag-AgCl (3M KCl); or a limit current density value of 0.25  $\text{mA cm}^{-2}$ .

Morphology and chemical composition of the corrosion product after polarisation tests were characterised by a Hitachi S 4800 J field emission scanning electron microscopy (FEG-SEM) equipped with Energy Dispersive X-Ray-EDX-Detector.

### Results and discussions

The investigated Bi-Zn solder alloys are indicated by dashed vertical lines in the partial phase diagram, calculated by the computational Thermodynamics Software – ThermoCalc®, shown in Figure 1, where images of the typical microstructures observed in the present study are also shown. As it can be seen, the alloys with different Zn content present distinct microstructural morphologies. The solidification of the hypoeutectic alloy (Bi-1.5wt-%Zn) does not have complex phase transformations. The primary phase formed is a Bi-rich pro-eutectic phase and the remaining liquid solidifies as a eutectic mixture. The Bi-rich phase solidified with a morphology, named as ‘trigonal dendrite’, with the interdendritic region composed by a eutectic mixture, characterised by Zn fibres disseminated into the Bi-rich phase. The dark phase corresponds to the Zn-rich primary phase of the eutectic mixture.

For the Bi-2.7 wt-% Zn eutectic alloy, the microstructure is entirely formed by the eutectic mixture. In the hypereutectic alloy (Bi-5wt-%Zn), the presence of pro-eutectic longer and thicker Zn fibres (as compared to those of the eutectic phase) non-homogeneously distributed in the eutectic matrix can be observed.

Aiming to evaluate the corrosion kinetics of these alloys, potentiodynamic polarisation tests were performed in alloy samples extracted from each directionally solidified alloy casting.

Figure 2 compares the polarisation curves corresponding to the pure elements, Bi and Zn. As it can be seen, they exhibit a different corrosion behaviour. First, pure bismuth presents a cathodic branch under activation control while the anodic branch shows a passive behaviour which displays a pitting potential at 300 mV vs. Ag/AgCl (3M KCl); while, pure zinc shows an anodic branch under activation control and a cathodic branch under diffusion control. Second, the corrosion potential is markedly different, about  $-0.185 \text{ V}$  and  $-1.05 \text{ V vs. Ag/AgCl (3M KCl)}$  for Bi and Zn, respectively. The difference from the kinetics point of view is also significant, since the corrosion current density corresponding to Zn is  $13 \mu\text{A cm}^{-2}$ , while to the passivation current to Bi is  $0.25 \mu\text{A cm}^{-2}$ . Therefore, this indicates that Bismuth presents a corrosion rate one order of magnitude lower than Zn.

The polarisation curves corresponding to the hypoeutectic, eutectic, and hypereutectic alloys are presented in Figure 3. All the samples show a diffusion control, characterised by vertical cathodic branch. As it can be seen, the polarisation curves for the Bi-Zn alloys show that the corrosion potential

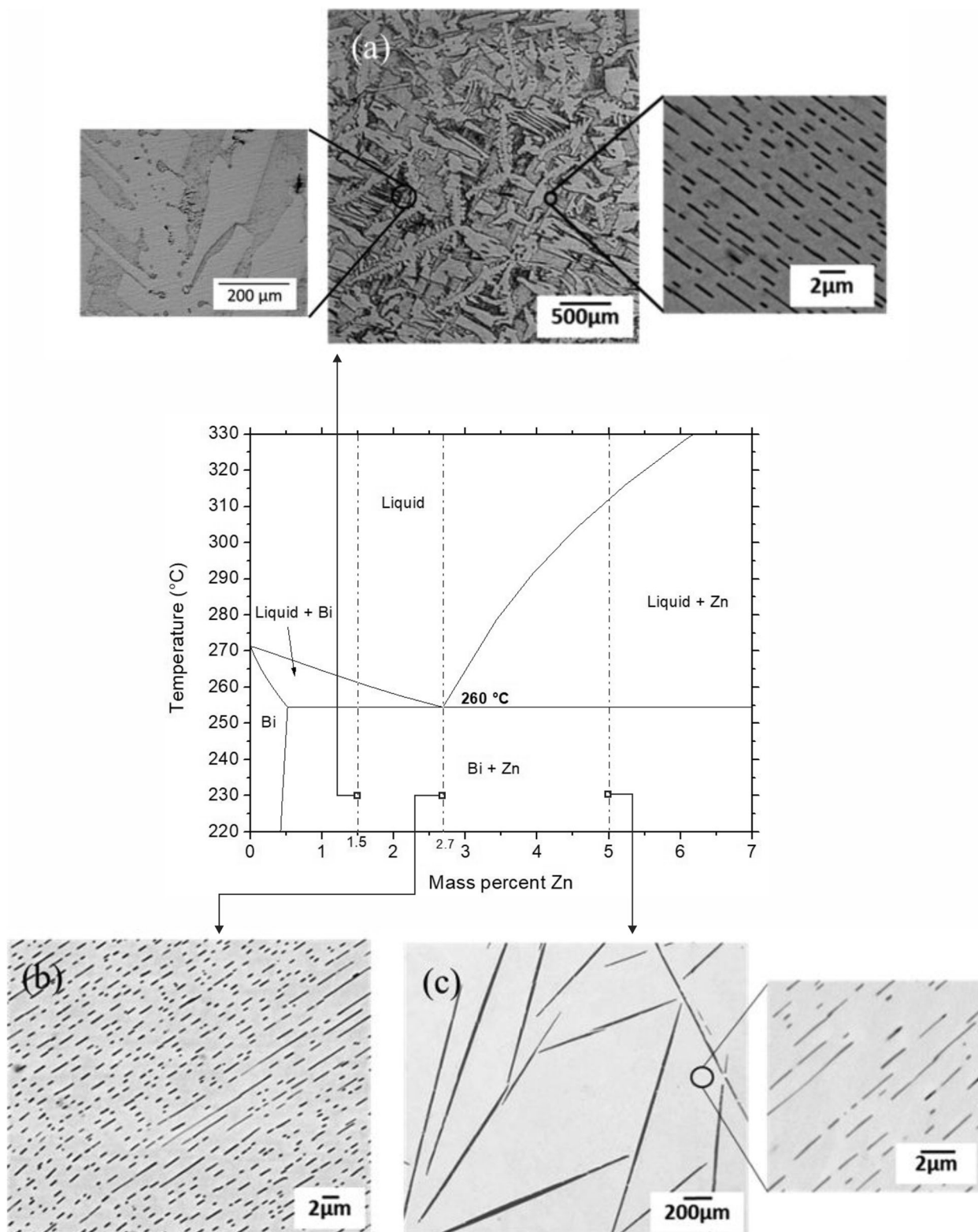


**Figure 1.** Partial binary Bi-Zn phase diagram and typical as-solidified microstructures of the examined alloys: (a) Bi-1.5wt-%Zn (b) Bi-2.7wt-%Zn and (c) Bi-5wt-%Zn.

in comparison to Bi shifts towards less noble values with increasing Zn content of the alloy. The limiting current density and corrosion potential described for the hypoeutectic and eutectic alloys (1.5 and 2.7wt-%, respectively) are similar:  $16 \mu\text{A cm}^{-2}$  and  $-0.75 \text{ V vs. Ag/AgCl}$ . The highest current density,  $32 \mu\text{A cm}^{-2}$ , corresponds to the hypereutectic Bi-5wt-% Zn alloy. An increase of Zn content increases the reactivity of Bi-Zn alloy and, thereby, the Bi-5wt-% Zn alloy presents the highest limiting current density. Although there is no particular difference, it is expected a greater degradation.

These results show that even small additions of Zn to Bi, cause the loss of its characteristic passivity and, accelerate its corrosive kinetics becoming the same order as that of pure Zn.

This activation of the corrosion kinetics regarding to pure Bi must be related to changes in the microstructure. It is well known that heterogeneities resulting from the formation of different phases in the metal matrix exhibit distinct corrosion behaviour and may lead to the formation of micro galvanic couples due to the potential difference between phases. As

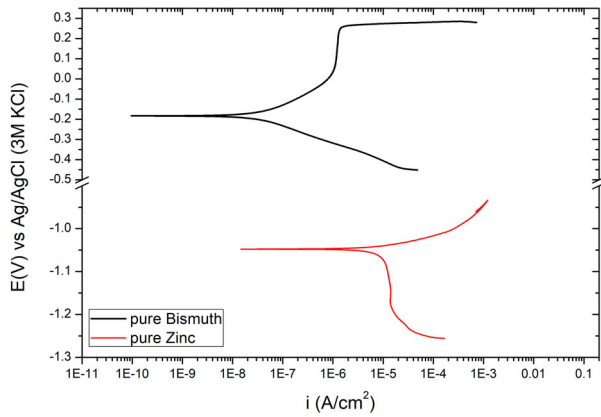


Figure 2. Polarisation curves of pure Bi and Zn in a 0.06 M NaCl solution.

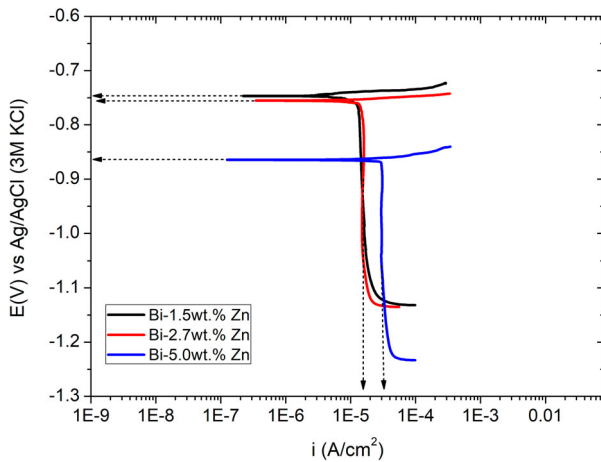
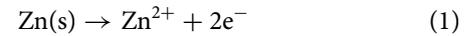


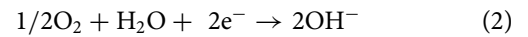
Figure 3. Polarisation curves of Bi-Zn alloy in 0.06 M NaCl.

already shown in Figure 1, the Bi-rich phase presents a nobler behaviour, and therefore, acts as a cathode enhancing the dissolution of the less noble phase. As a result, the galvanic interaction between Bi and Zn becomes a serious concern for Bi-Zn alloys. Therefore, the corrosion resistance of the alloys of this metallic system will depend on the presence of the Zn fibres acting as anodes and their distribution in the Bi-rich matrix. Anyway, in case of exposure to harsh environments

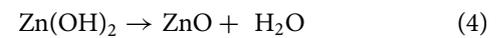
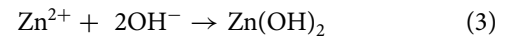
with the presence of high humidity and halide ions the susceptibility to corrosion arises [20] causing the preferential dissolution of the Zn-rich phase. Many works have been devoted to understand the zinc oxidation mechanism [21–24]. The corrosion process begins with the dissolution of zinc at anodic sites:



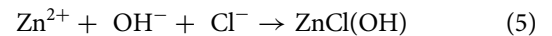
The electrons produced from the anodic reaction shown in (1) react with water and oxygen generating hydroxide anion at cathodic sites:



Subsequently, the anodic reaction produces ( $\text{Zn}^{2+}$ ) and the cathodic reaction ( $\text{OH}^-$ ) that reacts to form zinc hydroxide, which in turn dehydrate forming zinc oxide.



Chlorides do not stay adsorbed due to their high reaction rate with metals. Instead, they form soluble species that react, leading to accelerated corrosion [25]. As already reported [26], the presence of chlorides ions in the electrolyte activates the dissolution of the electrode, since zinc hydroxychloride is formed:



The layer composed by zinc oxide and zinc hydroxide is dissolved when reacting with chloride ions due to soluble nature of zinc hydroxychloride, provoking the exposition of the underlying zinc to the electrolyte and resulting into localised attack [26].

Figure 4 shows the SEM/BSE micrographs of the surface morphology of the Bi-1.5wt-% Zn alloy sample after the polarisation test. Bismuth presents high atomic density, consequently, it is identified as the large light phase, and the corrosion product is seen as the dark phase. As can also be seen, the corrosive attack occurs in the interdendritic phase (eutectic mixture, consisting of Zn-rich fibres disseminated in the Bi-rich phase), while the Bi-rich trigonal dendrites remain more preserved. It is worth noting that the Zn fibres are

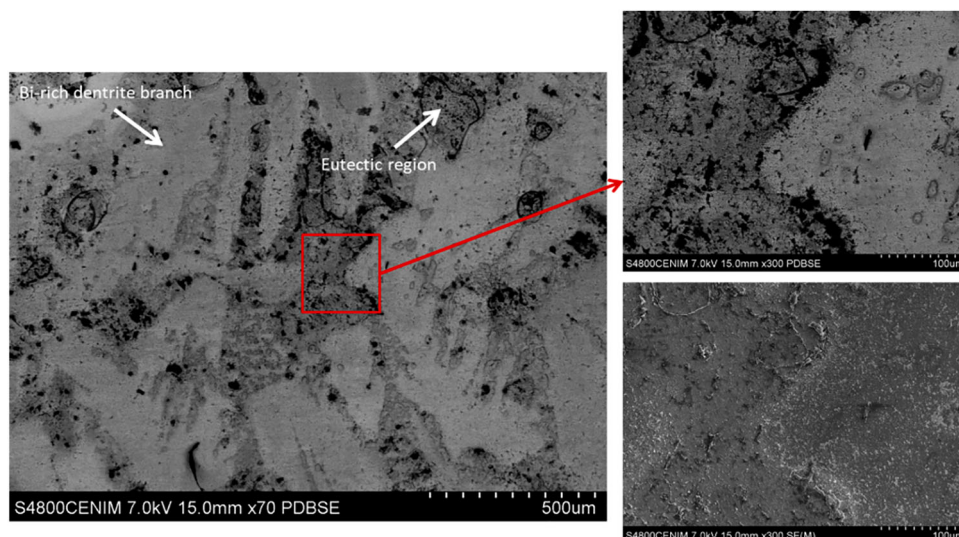


Figure 4. SEM/BSE images of a Bi-1.5wt-%Zn alloy sample after the corrosion test in a NaCl solution (0.06 M).

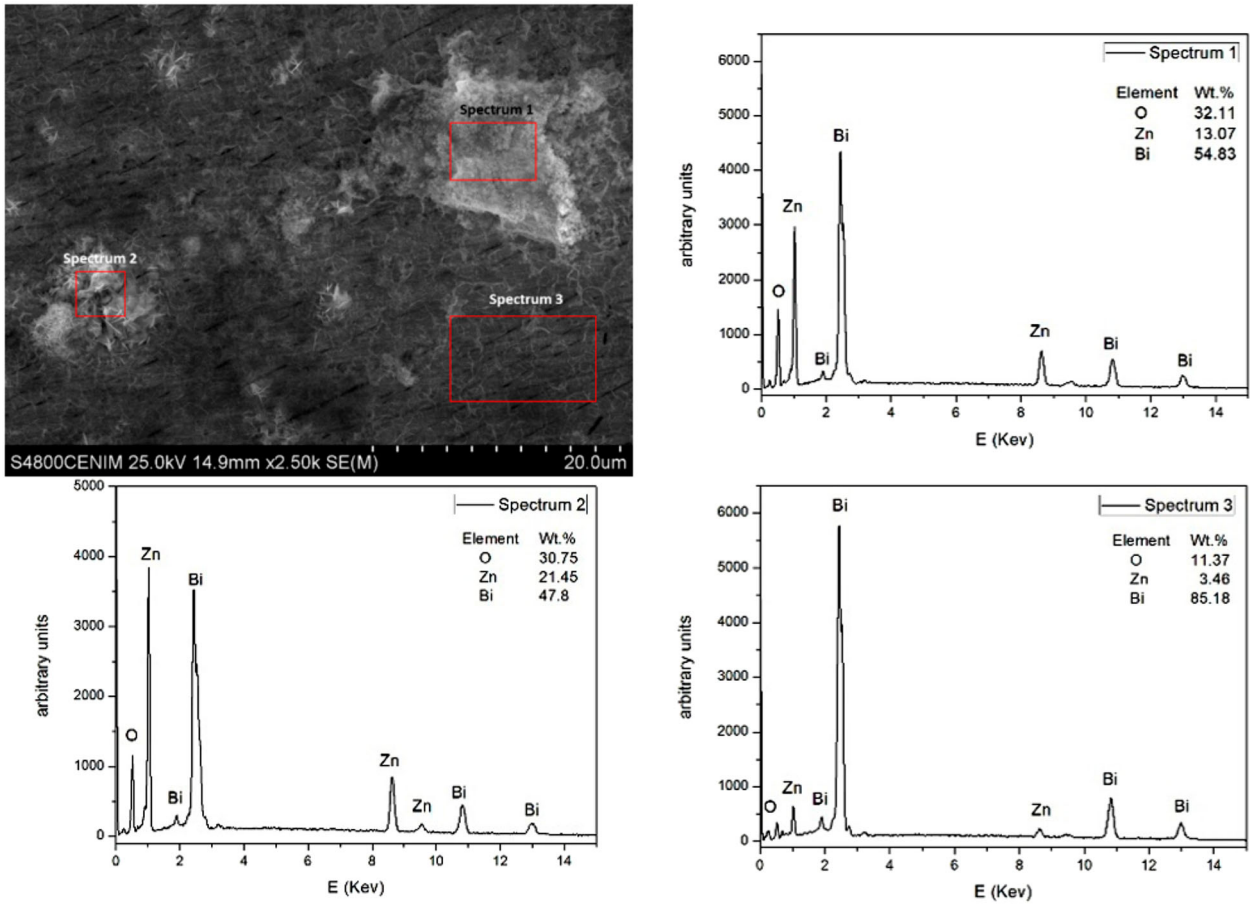


Figure 5. SEM/EDS images of oxidised areas in the Bi-1.5wt-%Zn alloy sample.

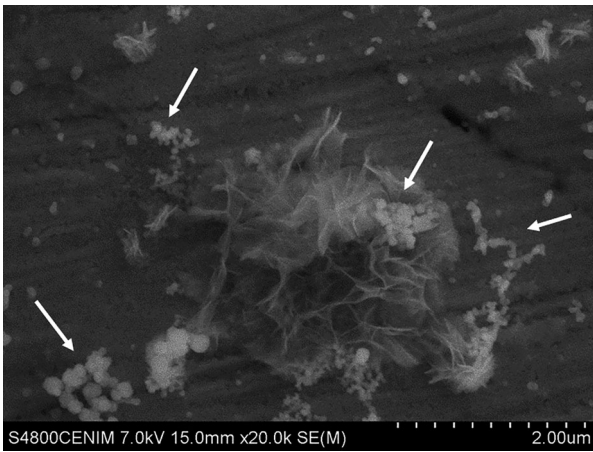


Figure 6. SEM image of ZnO areas found in the Bi-1.5wt-% alloy sample after the potentiodynamic polarisation test.

very small (approximately 1.18 µm), which does not allow their observation in the magnification of this image.

Figure 5 shows the interdendritic eutectic region, which is covered by an uneven oxide layer with whitish appearance. The spectra 1, 2 and 3 obtained through EDS analyses revealed that the product is ZnO, the intensity of the peaks related to this oxide is higher for the spectra obtained in the regions where the oxide layer is denser (spectra 1 and 2). In higher magnification (Figure 6), it is possible to identify two morphologies of the corrosion product: typical agglomerates with edge-like structure and very small agglomerates of spherical particles of diameter less than 0.2 µm.

The SEM micrographs of the surface of Bi-2.7wt-%Zn alloy samples after the polarisation test, shown in Figure 7, reveal a surface covered by a homogeneous film of ZnO. The oxide morphology presented by the eutectic alloy is the

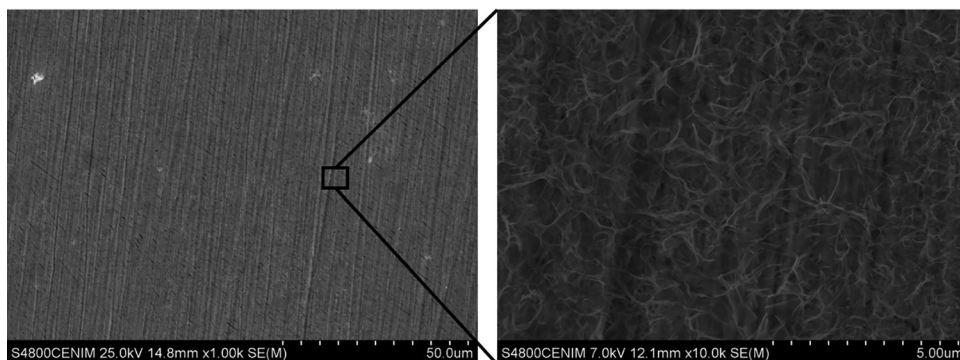
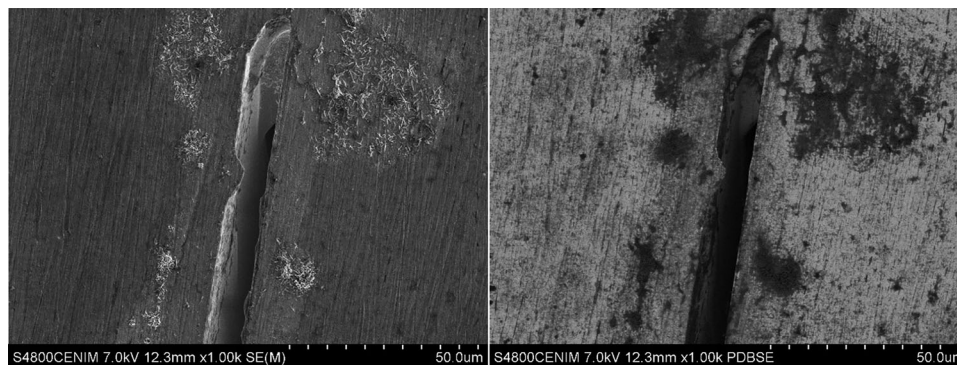


Figure 7. SEM micrograph (Secondary electron-SE) of a Bi-2.7wt-%Zn sample after the corrosion test.



**Figure 8.** SEM micrographs of the Bi-5.0wt-%Zn alloy sample after the corrosion test: (a) Secondary electron (SE) and (b) Backscattered electron (BE) imaging.

same presented by the hypoeutectic (edge-like structure), however, apparently the oxide is more homogeneous on the surface. It may be a result of the slight increase in the alloy zinc content, as well as of the better distribution of the phases in the microstructure of the alloy.

An increase in Zn content increases the reactivity of Bi-Zn alloys, thereby, the Bi-5wt-% Zn alloy presented the highest limiting current density observed in this work, and consequently, the highest degree of corrosion of the examined alloys. It can be noted in Figure 8 that pro-eutectic large and thick Zn fibres were preferentially dissolved, promoting selective attack inward the alloy sample.

## Conclusions

The corrosion resistance of Bi-*x*Zn (1.5, 2.7 and 5wt-%) solder alloys has been experimentally investigated by linear polarisation and surface analysis. The increase in the alloy Zn content promotes changes on the microstructural morphology, and consequently, on the corrosion behaviour of the examined Bi-Zn alloys, turning the passive behaviour of Bi into a diffusive behaviour of Zn. The Bi-5wt-% Zn alloy presented the highest limiting current density, and consequently, the highest degree of corrosion of the examined alloys. On the other hand, such higher content of Zn in the alloy reveal a corrosion mechanism dominated by the selective dissolution of the Zn needles.

The polarisation curves show that the corrosion potential is shifted towards less noble values with the increase in the alloy Zinc content to 5wt-%, which means that alloys with increasing Zn content can be more active in a 0.06M NaCl solution. The corrosion products are derived from the dissolution of Zinc with the formation of ZnO.

The surface analysis permitted to conclude that the oxide morphology presented by the eutectic alloy, an edge-like structure, is the same presented by the hypoeutectic alloy, however, apparently more uniform and compact, which may be related with the slight increase in the alloy zinc content, as well as with the better distribution of the phases presented in the alloy microstructure. For the hypereutectic alloy, the pro-eutectic large and thick Zn fibres are selectively and preferentially dissolved, promoting selective corrosion inward the alloy sample.

## Disclosure statement

No potential conflict of interest was reported by the authors.

## Funding

The authors are grateful to CAPES – Coordenação de Aperfeiçoamento de Pessoal de Nível Superior – Brasil (Finance Code 001- grant: 88881.135396/2016-01), CNPq – National Council for Scientific and Technological Development (grant: 408576/2016-2) and FAPESP – São Paulo Research Foundation (grants: 2017/15158-0 and 2017/16058-9), for their financial support.

## ORCID

Rudimylla S. Septimio  <http://orcid.org/0000-0002-5816-8821>  
 Maria A. Arenas  <http://orcid.org/0000-0002-7807-8209>  
 Ana Conde  <http://orcid.org/0000-0001-7889-8664>  
 Amauri Garcia  <http://orcid.org/0000-0002-3834-3258>  
 Noé Cheung  <http://orcid.org/0000-0003-1120-8926>  
 Juan de Damborenea  <http://orcid.org/0000-0002-8053-594X>

## References

- [1] Krenev VA, Drobot NF, Fomichev SV. Bismuth: reserves, applications, and the world market. *Theor Found Chem Eng.* 2015;49:532–535.
- [2] Leonard N, Wieland L, Mohan R. Applications of bismuth (III) compounds in organic synthesis. *Tetrahedron.* 2002;58:8373–8397.
- [3] Poudel B, Hao Q, Ma Y, et al. High-thermoelectric performance of nanostructured bismuth antimony telluride bulk alloys. *Science.* 2008;320:634–638.
- [4] Nayek P, Li G. Superior electro-optic response in multiferroic bismuth ferrite nanoparticle doped nematic liquid crystal device. *Sci Rep.* 2015;5:1–9.
- [5] Đuran I, Entler S, Kocan M, et al. Development of bismuth hall sensors for ITER steady state magnetic diagnostics. *Fusion Eng Des.* 2017;123:690–694.
- [6] Yu T, Lu S, Xu W, et al. Fabrication of bismuth superhydrophobic surface on zinc substrate. *J Solid State Chem.* 2018;262:6–37.
- [7] Freitas ES, Silva AP, Spinelli JE, et al. Inter-relation of microstructural features and dry sliding wear behavior of monotectic Al-Bi and Al-Pb alloys. *Tribol Lett.* 2014;55:111–120.
- [8] Costa TA, Dias M, Freitas ES, et al. The effect of microstructure length scale on dry sliding wear behaviour of monotectic Al-Bi-Sn alloys. *J Alloys Compd.* 2016;689:767–776.
- [9] Suganuma K, Kim SJ, Kim KS. High-temperature lead-free solders: properties and possibilities. *JOM.-J Met.* 2009;61:64–71.
- [10] Liu JC, Wang ZH, Xie JY, et al. Understanding corrosion mechanism of Sn-Zn alloys in NaCl solution via corrosion products characterization. *Mater Corros.* 2016;67:522–530.
- [11] Osório WR, Garcia LR, Peixoto LC, et al. Electrochemical behavior of a lead-free SnAg solder alloy affected by the microstructure array. *Mater Des.* 2011;32:4763–4772.
- [12] Osório WR, Spinelli JE, Afonso CRM, et al. Microstructure, corrosion behaviour and microhardness of a directionally solidified Sn-Cu solder alloy. *Electrochim Acta.* 2011;56:8891–8899.

- [13] Osório WR, Freire CM, Caram R, et al. The role of Cu-based intermetallics on the pitting corrosion behavior of Sn-Cu, Ti-Cu and Al-Cu alloys. *Electrochim Acta*. 2012;77:189–197.
- [14] Zhongbo Y, Zhuqing C, Jun Q, et al. Correlation between microstructure and corrosion behavior of Zr-0.8Sn-1Nb-0.3Fe alloy. *Rare Met Mater Eng*. 2018;47:794–798.
- [15] Brito C, Vida T, Freitas E, et al. Cellular/dendritic arrays and intermetallic phases affecting corrosion and mechanical resistances of an Al-Mg-Si alloy. *J Alloys Compd*. 2016;673:220–230.
- [16] Verissimo NC, Freitas ES, Cheung N, et al. The effects of Zn segregation and microstructure length scale on the corrosion behavior of a directionally solidified Mg-25 wt-%Zn alloy. *J Alloys Compd*. 2017;723:649–660.
- [17] Ahmido A, Sabbar A, Zouihri H, et al. Effect of bismuth and silver on the corrosion behavior of Sn-9Zn alloy in NaCl 3wt.% solution. *Mater Sci Eng B Solid-State Mater Adv Technol*. 2011;176:1032–1036.
- [18] Vida TA, Conde A, Freitas ES, et al. Directionally solidified dilute Zn-Mg alloys: correlation between microstructure and corrosion properties. *J Alloys Compd*. 2017;723:536–547.
- [19] Septimio RS, Costa TA, Vida TA, et al. Interrelationship of thermal parameters, microstructure and microhardness of directionally solidified Bi-Zn solder alloys. *Microelectron Reliab*. 2017;78:100–110.
- [20] Mouanga M, Berçot P. Comparison of corrosion behaviour of zinc in NaCl and in NaOH solutions; Part II: electrochemical analyses. *Corros. Sci*. 2010;52:3993–4000.
- [21] Touri F. Detection and characterization of ZnO on a passive film of pure zinc. *Int J Electrochem Sci*. 2017;12:10813–10823.
- [22] Baugh LM, Baikie AR. Passivation of zinc in concentrated alkaline solution-II. Role of various experimental factors and the distinction between the solid-state and dissolution-precipitation mechanisms. *Electrochim Acta*. 1985;30:1173–1183.
- [23] Baugh LM, Higginson A. Passivation of zinc in concentrated alkaline solution-I. Characteristics of active dissolution prior to passivation. *Electrochim Acta*. 1985;30:1163–1172.
- [24] Ye C, Fang X, Hao Y, et al. Zinc oxide nanostructures: morphology derivation and evolution. *J Phys Chem B*. 2005;109:19758–19765.
- [25] Foley RT. Role of the chloride ion in iron corrosion. *Corrosion*. 1970;26:58–70.
- [26] Arenas MA, Damborenea J. Use of electrochemical impedance spectroscopy to study corrosion of galvanised steel in 0.6M NaCl solution. *Corros Eng Sci Technol*. 2006;41:228–234.

Copyright of Corrosion Engineering, Science & Technology is the property of Taylor & Francis Ltd and its content may not be copied or emailed to multiple sites or posted to a listserv without the copyright holder's express written permission. However, users may print, download, or email articles for individual use.